

## Article

# Regional-Scale Distribution of Helium Isotopes in Aquifers: How Informative Are They as Groundwater Tracers and Chronometers?

Daniele Luigi Pinti <sup>1,\*</sup>, Marie Larocque <sup>1</sup>, Pauline Méjean <sup>2</sup>, Marion Saby <sup>1</sup>, Mario Alberto Hernández-Hernández <sup>3</sup>, Sylvain Gagné <sup>1</sup>, Emilie Roulleau <sup>4</sup>, Yuji Sano <sup>5</sup>, Maria Clara Castro <sup>6</sup>, Takuya Matsumoto <sup>7</sup> and Viorel Horoi <sup>1</sup>

<sup>1</sup> Geotop & Département des Sciences de la Terre et de l'Atmosphère, Université du Québec à Montréal, Montréal, QC H3C 3P8, Canada; larocque.marie@uqam.ca (M.L.); saby.marion.e@gmail.com (M.S.); gagne.sylvain@uqam.ca (S.G.); horoi.viorel@uqam.ca (V.H.)

<sup>2</sup> Géosciences Environnement Toulouse, CNRS, Observatoire Midi Pyrénées, UMR 5563, 31400 Toulouse, France; pauline.mejean@get.omp.eu

<sup>3</sup> Cátedras CONACyT-Instituto de Geofísica, UNAM, Circuito de la Investigación Científica s/n, C.U., Ciudad de Mexico 04150, Mexico; albertohh@live.com

<sup>4</sup> STRATAGEM974, 62 Boulevard du Chaudron, 97490 Sainte-Clotilde, France; roulleau@stratagem974.com

<sup>5</sup> Center for Advanced Marine Core Research, Kochi University, Kochi 783-8502, Japan; yuji.sano@kochi-u.ac.jp

<sup>6</sup> Department of Earth and Environmental Sciences, University of Michigan, Ann Arbor, MI 48109-1005, USA; mccaastro@umich.edu

<sup>7</sup> Isotope Hydrology Section, Division of Physical and Chemical Sciences, IAEA, 1400 Vienna, Austria; t.matsumoto@iaea.org

\* Correspondence: pinti.daniele@uqam.ca; Tel.: +1-514-987-3000 (ext. 2572)



**Citation:** Pinti, D.L.; Larocque, M.; Méjean, P.; Saby, M.; Hernández-Hernández, M.A.; Gagné, S.; Roulleau, E.; Sano, Y.; Castro, M.C.; Matsumoto, T.; et al. Regional-Scale Distribution of Helium Isotopes in Aquifers: How Informative Are They as Groundwater Tracers and Chronometers? *Water* **2022**, *14*, 1940. <https://doi.org/10.3390/w14121940>

Academic Editor:  
Giovanni Martinelli

Received: 10 April 2022

Accepted: 14 June 2022

Published: 16 June 2022

**Publisher's Note:** MDPI stays neutral with regard to jurisdictional claims in published maps and institutional affiliations.



**Copyright:** © 2022 by the authors. Licensee MDPI, Basel, Switzerland. This article is an open access article distributed under the terms and conditions of the Creative Commons Attribution (CC BY) license (<https://creativecommons.org/licenses/by/4.0/>).

**Abstract:** This study presents an almost entirely unpublished dataset of 121 samples of groundwater analyzed for helium concentration and its isotopic ratio ( $^3\text{He}/^4\text{He}$ ) in two adjacent watersheds of the St. Lawrence Lowlands, in a region with intensive agricultural activities in the southern Québec Province, Eastern Canada. Most of the samples were collected in the regional bedrock fractured aquifer hosted in mid-Ordovician siliciclastic shales, on a total surface of 7500 km<sup>2</sup>. Even with this low-density sampling, and in a heterogeneous and fractured aquifer, the helium isotopes bring precious information on the recharge conditions and on chemical evolution of water. The helium spatial interpolation does not show a clear isotopic gradient through the basin. However, it shows progressive enrichment of radiogenic  $^4\text{He}$  in the confined part of the aquifer. The atmospheric and/or tritogenic-rich helium occurs at the recharge in the Appalachians and in the middle of the plain, where impermeable cover is limited, and local infiltration of meteoric freshwater reaches the bedrock aquifer. The relation between the total dissolved solids (TDS) and  $^3\text{He}/^4\text{He}$  ratios remains elusive. However, on discriminating the samples with the dominant chemistry of water, a clear trend is observed with  $^3\text{He}/^4\text{He}$  ratio, suggesting that radiogenic  $^4\text{He}$  accumulates together with dissolved solids and with increasing time (indicated by progressively older  $^{14}\text{C}$  ages). Finally, the noble gas temperatures (NGTs) obtained from concentrations of the other noble gases (Ne, Ar, Kr and Xe) brings constraints on the earlier recharge conditions during the Holocene. Particularly, the NGTs showed that the studied aquifers were continuously replenished, even under ice-sheet cover in the last 10,000 years.

**Keywords:** recharge; groundwater age; helium isotopes;  $^{14}\text{C}$ ; noble gas paleotemperatures

## 1. Introduction

The helium isotopes ( $^3\text{He}$  and  $^4\text{He}$ ) have been widely used to trace sources of water in a diversity of geological settings, from shallow groundwater (e.g., [1–5]), to basinal brines [6–9]. This is because helium and all of the other noble gases (Ne, Ar, Kr and

Xe) are chemically inert. As such, their isotopic signature is not modified by water–rock interactions, rather, it reflects the original fluid sources in which they were dissolved.

The noble gases possess two other characteristics which are not present in classical tracers used in hydrology, such as the stable isotopes of water ( $\delta^2\text{H}$  and  $\delta^{18}\text{O}$ ). First, they can be used to estimate the groundwater residence times, due to the presence of isotopes produced by the decay of short-lived nuclides such as  $^3\text{H}$ —which produces  $^3\text{He}$  [10]—and  $^{235}\text{U}$ ,  $^{238}\text{U}$  and  $^{232}\text{Th}$ —which produces  $^4\text{He}$  [11,12]. The accumulation rate of these radiogenic isotopes in fluids might provide constraints on the mean residence time of the groundwater in an aquifer, both in the modern realm (the  $^3\text{H}/^3\text{He}$  method can be used in the ~0–80 years old range), and in the distant past, from thousands to billions of years ago [8,13,14]. The second characteristic is the temperature dependency of their solubilities in groundwater. Therefore, the atmospheric noble gases (ANG) dissolve at the water table level with concentrations reflecting the current ambient temperature (equilibrium dissolution following Henri’s law [15]). Their inert nature ensures the preservation of this initial concentration—which is defined as ASW or Air Saturated Water—over time. The preservation of these original concentrations of ANG in old waters allows for the reconstruction of past climates. The heavier noble gases (Ar, Kr, Xe) are particularly sensitive to temperature changes and paleoclimate reconstructions are based mostly on these concentrations of noble gas [16–19]. Therefore, they can be used to obtain subtle information on the past climatic conditions of the recharge, particularly if the recharge was functioning during glaciated periods, which punctuated the Quaternary and modified the aquifers’ dynamics and recharge conditions [18,20–22].

This contribution reports on helium isotopes obtained from the fractured regional aquifers of southern Québec (Figure 1a). Over the last decade, numerous hydrogeochemical studies funded by the Québec provincial government (PACES—*Programme d’acquisition de connaissances des eaux souterraines*) were carried out in this region (e.g., [23–26]). The goal of this extended research program was to paint a portrait of the water resources available in the Québec Province, particularly in this central region, where most of the agricultural production is concentrated and where the groundwater is used for irrigation, industry and locally as a source of drinking water.

The goal of this specific study is to couple at a regional scale the helium isotopic signature of groundwater with other age tracers ( $^3\text{H}/^3\text{He}$  and  $^{14}\text{C}$ ) and dissolved ions to provide an integrated and novel understanding of the conceptual regional groundwater circulation model. This, in turn, will allow for a clearer assessment of the benefits and limitations of noble gases as natural water tracers and chronometers at a basin scale.

Extensive isotopic surveys, including the noble gases of the Bécancour (BEC) and Nicolet/Lower Saint-François (NSF) neighboring watershed regions (Figure 1a), were carried out by our research group, but only a limited quantity of the noble gas data was published [27] or discussed [28]. The published data include 30 helium isotopic ratios and 19 noble gas temperatures from the BEC aquifers. A total of 121 items of helium data (six duplicates), including the 30 measurements from [27], obtained from the 115 wells sampled in the two regions of BEC and NSF, together with 28 noble gas-derived water table paleotemperatures, are presented and discussed (Tables S1 and S2, Supplementary Materials).

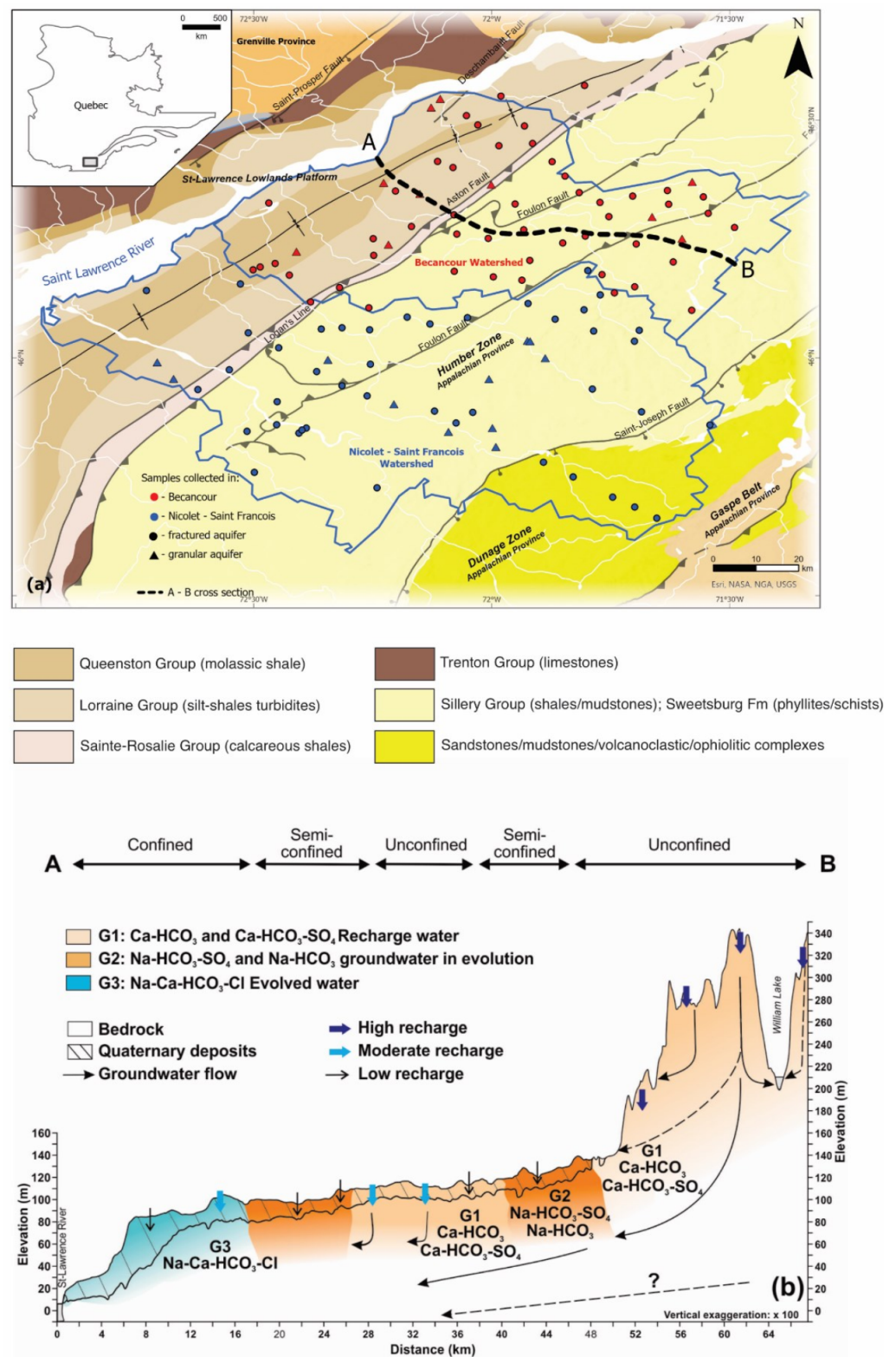


**Figure 1.** (a) Location of the studied region within the St. Lawrence Lowlands, with the geology of the bedrock fractured aquifer and main faults. The position of sampled wells in Quaternary granular (triangles) and mid-Ordovician bedrock fractured (circles) aquifers is reported. Samples collected in the Bécancour (BEC) watershed are in red and those of the Nicolet/Lower St-François (NSF) watershed are in blue; (b) Schematic cross-section through the Bécancour watershed, illustrating the chemical evolution of water along the flow path.

## 2. Materials and Methods

### 2.1. Study Area

The NSF (4500 km<sup>2</sup>) and BEC (2859 km<sup>2</sup>) watersheds occupy the central part of the St. Lawrence Lowlands (Figure 1a). The study area overlaps the two distinct geological provinces of southern Québec, namely the St. Lawrence Platform and the Appalachian Mountains (Figure 1a). The St. Lawrence Platform consists of a 1200 m-thick Cambrian–Lower Ordovician siliciclastic and carbonate platform formed during the opening of the Iapetus Ocean, between Laurentia and Baltica-Avalonia (e.g., [29]). It is overlain by ca. 1800 m of Mid–Late Ordovician foreland carbonate-clastic deposits, derived from the closure of this ocean and the formation of the Appalachian Mountains during the Taconic orogeny (480–440 Ma ago) [30]. The St. Lawrence Platform and the Appalachian provinces are separated by the low-angle Logan’s Line, also called the Logan’s Fault [31], which is a southeasterly dipping major thrust fault in northeastern and eastern North America, related to the culmination of the Taconic orogeny. The area is also crossed by other faults: steeply dipping, normal faults close to the St-Lawrence River and related to the opening of the St-Lawrence Rift System at the end of Paleozoic (e.g., the Deschambault Fault; Figure 1a); and a series of thrust and normal faults on the Appalachian Mts. (the Foulon and the St-Joseph faults, respectively; Figure 1a) [30,32].

The main lithologies composing the regional bedrock fractured aquifer are turbiditic carbonate and silt-shales of the Mid-Late Ordovician Lorraine and San Rosalie Groups, molassic red shales of the Queenston Group of the St. Lawrence Platform, and shales, calcitic schists [29] and phyllites mixed with the volcanoclastic material of Cambrian–Ordovician age from the metasedimentary sequences of the Appalachian Mountains (Figure 1a) [33]. The unconsolidated Quaternary sediments, including till units and fluvio-glacial sands derived from the last two glaciation–deglaciation cycles, unconformably cover the Cambrian–Ordovician sedimentary basal sequences [34]. The sedimentary sequences, comprising the fractured and granular aquifers, are not very deformed; generally, the strata are sub horizontal (max 5–10 °C dip), even in the northernmost portion of the studied area where the strata form the low angle Chambly-Fortierville Syncline (the brownish colored area in Figure 1a) [29]. Larocque et al. [24,25] did not identify any hydrogeological influence of the faults. Malgrange and Gleeson [35] also showed the limited influence of the Appalachian fault system on the local hydrogeology.

During the last deglaciation, the retreat of the Laurentide Ice Sheet caused a marine invasion from the Gulf of St. Lawrence, referred to as the Champlain Sea episode [36]. During this episode, glacio-marine and deltaic clays and sand patches were deposited, the former creating semi-confined conditions for some of the granular aquifers. Two main aquifer systems exist in the study area: (1) a spatially discontinuous and locally perched granular aquifer composed of a wide range of Quaternary deposits, ranging from fluvio-glacial sand and gravel to littoral fine sand with average thickness of 30 m [24,25,31]; and (2) a regional bedrock fractured aquifer in the Mid–Late Ordovician sedimentary units of the St. Lawrence Platform (Figure 1b). The regional aquifer consists of fractured bedrock of low to moderate ( $\sim 10^{-5}$ – $10^{-6}$  m/s) hydraulic conductivity. The wells in the rock aquifer yield enough water to supply single family dwellings and, in a few areas, small- to medium-size municipalities [31].

The recharge of the regional bedrock fractured aquifer is estimated to occur mainly in the southeastern Appalachian Mountains (Figure 1b) [24,25]. However, local recharge also occurs in the semi-confined conditions along the Appalachian piedmont and in the middle of the St. Lawrence plain (Figure 1b), disrupting any regional trend in water chemistry and age [27], and making it difficult to evaluate the groundwater flow at the basin-scale [37]. The recharge peaks occur following the spring snowmelt (April–May) and in the fall (October–November) [24,25,38]. The groundwater discharges into the numerous streams and rivers that are part of these watersheds and directly into the St. Lawrence River (Figure 1a) [37].

Based on their chemistry, four water types were identified in the study area: Ca-HCO<sub>3</sub>; Ca-Na-SO<sub>4</sub>; Na-HCO<sub>3</sub>; and Na-HCO<sub>3</sub>-Cl [39]. Following earlier studies by Cloutier et al. [40,41], a detailed conceptual model of the evolution of the St. Lawrence Lowlands' groundwater system was proposed (Figure 1b). In this model, the lithology of the Appalachians, where most of the recharge occurs, is mainly Ordovician carbonate-rich shales and Cambrian carbonate meta-sediments, yielding a Ca-HCO<sub>3</sub> and Ca-HCO<sub>3</sub>-SO<sub>4</sub> freshwater chemistry. Toward the central section of the St. Lawrence Lowlands, the groundwater evolves to Na-HCO<sub>3</sub> and Na-HCO<sub>3</sub>-SO<sub>4</sub> types, because the Ca<sup>2+</sup> dissolved in water exchanges with Na<sup>+</sup> in the mineral substrate (i.e., cationic exchange) [40]. Closer to the St. Lawrence River, the groundwater becomes slightly mineralized to Ca-HCO<sub>3</sub>-Cl, Na and Na-HCO<sub>3</sub>-Cl types, with chlorine derived from the saline pore water originating from the Champlain Sea marine transgression (Figure 1b) [41].

The radiocarbon (<sup>14</sup>C) and tritium (<sup>3</sup>H) ages validate this conceptual model of the groundwater's geochemical evolution, indicating the presence of two water types: (1) tritium-rich modern water in unconfined sections of the fractured Ordovician aquifer and in the unconsolidated Quaternary aquifer; and (2) tritium-free water with <sup>14</sup>C post-glacial ages younger than 13,000 years in the confined fractured bedrock aquifer [26,27,37,41].

## 2.2. Analytical Methods

The sampling techniques and analytical methods employed to measure the noble gases in the groundwater are briefly described here. Detailed descriptions can be found in [27,28].

Of the 320 samples collected for the major and minor ion analysis in the BEC and NSF regions between 2010 and 2013 through the PACES program, 121 groundwater samples were collected from 115 municipal and private wells and observation piezometers were analyzed for noble gases (Figure 1a; Table S1, Supplementary Materials). Only 22 of the wells tapped in the unconsolidated (granular) Quaternary aquifer; the remaining ones are open borehole wells that tap water from the carbonate-shale-dominated mid-Ordovician fractured aquifer system (Table S1, Supplementary Materials). Twelve piezometers were drilled and instrumented for monitoring purposes during the PACES project [24,25] (BEC-R and NSF-R prefixes in Table S1 (Supplementary Materials)). The median well depth of the granular aquifer in the studied area is 14 m. That of the fractured aquifer is 40 m [37]. The limited depth of the wells in the fractured rock reflects the rapidly decreasing density of fractures (and hydraulic conductivity) with depth [31].

The groundwater was collected from the instrumented piezometers for noble gas measurements using a Waterra<sup>®</sup> Inertial Pump System, which consists of a foot valve fixed to the bottom of a high-density polyethylene tube with a variable diameter of 5/8" to 2", and an electric Hydrolift-2<sup>®</sup> actuator pump. The water from the municipal wells was collected at the wellhead, and from the closest water faucet for domestic wells, to avoid intermediate tanks where the water could degas and/or mix with inhibitor chemicals. The water was purged from the wells and piezometers until chemo-physical parameters (i.e., fluid electrical conductivity, pH, Eh and fluid temperature) stabilized. The water was subsequently allowed to flow through armored PVC tubes connected to 3/8"-diameter refrigeration-type copper tubes with stainless-steel clamps at both extremities. After a few minutes, two steel clamps were sealed using electric drills and the sealed tube recovered for noble gas analyses.

The noble gases were measured at two different laboratories: the Noble Gas Laboratory of the University of Michigan and the Marine Analytical Chemistry Laboratory of the University of Tokyo Ocean and Atmospheric Research Institute. At the University of Michigan, after extraction and purification on getters, He, Ne, Ar, Kr and Xe were sequentially inlet into a MAP 215-50 mass spectrometer equipped with a Faraday detector and an electron multiplier in ion-counting mode. Prior to each sample analysis, a calibrated amount of air standard was analyzed and the isotopic abundances for each sample were normalized to the air standard after blank correction. The elemental abundances of He,

Ne, Ar, Kr and Xe have typical uncertainties of 1.5, 1.3, 1.3, 1.5 and 2.2%, respectively. The additional details on the noble gas analytical procedures can be found in [42]. At the University of Tokyo, the samples were degassed and collected in a lead-rich glass ampoule. The ampoule was then connected to a stainless-steel line for purification on a Ti-getter and for the cryogenic separation of He from other noble gases. The helium aliquot was then analyzed for the  $^3\text{He}/^4\text{He}$  isotopic ratio using a Helix SFT calibrated against the helium standard of Japan (HESJ standard; [43]). The precision of the HESJ  $^3\text{He}/^4\text{He}$  ratio is typically  $\pm 0.2\%$  ( $2\sigma$ ). Prior to being cryogenically adsorbed, the amount of  $^{20}\text{Ne}$  was measured on a Pfeiffer Balzers QMS Prisma 80 (Pfeiffer Vacuum, Aslar, Germany) connected to the preparation line.

The noble gas temperatures (NGTs) were determined for BEC (data from [27]) and for NSF (unpublished data). These are based on interactive models, where the concentrations of the atmospheric noble gases Ne, Ar, Kr and Xe (which should be at ASW conditions and thus dependent on the recharge soil temperature) are corrected for degassing and excess air addition, for which a common temperature and smallest deviation is achieved [44]. The NGTs were calculated using the unfractionated air model, implemented in the inverse method of [45]. The model allows the amount of excess air to be estimated, which results from air bubbles entering the surface water table and subsequently dissolving in the groundwater [46].

The water samples for tritium analysis were collected using 1 L Nalgene<sup>®</sup> bottles, filled and sealed before shipment to the Environmental Isotope Laboratory of the University of Waterloo, where liquid scintillation counting is used to quantify tritium. The samples were enriched 15 times by electrolysis before counting. The detection limit for the enriched samples is 0.8 TU.

The graphite sources for  $^{14}\text{C}$  analyses in the BEC water samples were prepared from pure  $\text{CO}_2$  fractions at the Université de Paris Sud, and the sources were measured by accelerator mass spectrometry (the ARTEMIS accelerator of the UMS LMC14 of INSU-CNRS, Gif-sur-Yvette, France; [27]). The  $^{14}\text{C}$  for the NSF samples were analyzed at the Beta Analytic Inc. Laboratory, Florida, using a Single Stage Accelerator Mass Spectrometer (SSAMS) [28]. The  $^{14}\text{C}$  content is expressed as a percentage of modern carbon (pMC). The corrected  $^{14}\text{C}$  ages were determined by [28], using the correction method of [47]. Vautour et al. [27] were asked to recalculate the  $^{14}\text{C}$  corrected ages using NETPATH software [48]. This correction method is valid only for a series of wells located along the same flow path, in an aquifer in which the flow behaves as a piston-flow model. This is not the case in the studied area, and, as a result, it is likely that  $^{14}\text{C}$  ages in the BEC watershed were over-corrected in some of the samples. For consistency with the  $^{14}\text{C}$  ages previously obtained in the NSF by [28], all of the BEC  $^{14}\text{C}$  ages were recalculated, following [47]. These are reported in Table S1 (Supplementary Materials).

### 3. Results and Discussion

Table S1 (Supplementary Materials) reports all of the sampled wells and piezometers with coordinates WGM84, well depth, altitude, TDS, the chemical type (the latter subdivision based on the work of [39]),  $^4\text{He}$  content (in  $\text{cm}^3\text{STP/g}$ ),  $^4\text{He}/^{20}\text{Ne}$  ratios and the  $^3\text{He}/^4\text{He}$  ratios, normalized to the atmospheric ratio ( $R_a = 1.384 \times 10^{-6}$ , [49]) or  $R/R_a$ . The  $^3\text{H}/^3\text{He}$  apparent ages and  $^{14}\text{C}$  corrected ages (based on the model of [47]) are recalculated from the  $^3\text{H}$  and  $^{14}\text{C}$  activities reported by [27] and [28]. In Table S2 (Supplementary Materials), the noble gas-calculated paleotemperatures (in  $^\circ\text{C}$ ) and the  $\Delta\text{Ne}$  (%) are reported. The  $\Delta\text{Ne}$  (%) (given as  $[\text{Ne}]_{\text{measured}}/[\text{Ne}]_{\text{ASW}} - 1 \times 100$ ; Table S2, Supplementary Materials) reflects the amount of this excess air. The calculated NGTs range from  $-0.75 \pm 3.91$   $^\circ\text{C}$  to  $+14.42 \pm 3.2$   $^\circ\text{C}$  (Table S2, Supplementary Materials).

The TDS (total dissolved solids) range from 27 to over 17,000 mg/L, with most of the values ranging between 72 and 184 mg/L. Three samples display extremely high salinity values, partly due to deicing salt contamination [28].

The  $^4\text{He}$  concentrations range from  $8.82 \times 10^{-10}$  to  $4.45 \times 10^{-6}$   $\text{cm}^3\text{STP/g}$ , with 25% of the values (first quartile or Q1) below  $6.65 \times 10^{-8}$   $\text{cm}^3\text{STP/g}$ , a value close to the expected threshold of  $4.75 \times 10^{-8}$   $\text{cm}^3\text{STP/g}$  corresponding to the expected atmospheric helium content (ASW) at the average MAAT (Mean Annual Air Temperature) of  $10^\circ\text{C}$ . A total of 75% of the measured values (third quartile or Q3) are below  $8.51 \times 10^{-7}$   $\text{cm}^3\text{STP/g}$ . Only a handful of the samples display  $^4\text{He}$  contents greater than  $1 \times 10^{-6}$   $\text{cm}^3\text{STP/g}$ , in particular the anomalous samples BEC101, BEC126 and NSF-R8. These anomalous enrichments are discussed below. The  $^4\text{He}/^{20}\text{Ne}$  ratios range from 0.11, lower than the expected ASW value at  $10^\circ\text{C}$  (0.276; [50]) to 159. The former points to degassing while the latter points to a minor impact of atmospheric helium in the mixture. Finally, the R/Ra values range from 0.015 to 4.57 with Q1 value of 0.24 and a Q3 value of 1.05.

The presence of the measurable tritium ( $^3\text{H}$ ) and radiocarbon ( $^{14}\text{C}$ ) in the groundwater indicate, as often observed in other hydrogeological systems, that the water is a mixture of a young, modern source and a much older one. The ages of the younger component identified through measurable tritium ( $^3\text{H}/^3\text{He}$  apparent ages computed by [27,28]), range from 2 years for a very shallow sample from the Quaternary granular aquifer (BEC118; Table S1, Supplementary Materials) to 88 years for sample BEC126, the most anomalous sample in terms of the radiogenic  $^4\text{He}$  content. The older water component displays  $^{14}\text{C}$  ages, varying from modern to 17,050 years (NSFR-1; Table S1, Supplementary Materials).

### 3.1. Helium Sources

The classical ‘‘Craig’s plot’’, where the  $^4\text{He}/^{20}\text{Ne}$  ratios are plotted against R/Ra ratios (Figure 2) [51], provides a straightforward identification of the helium sources in terrestrial fluids, as well as the occurrence of mixing, usually represented by hyperbolas.

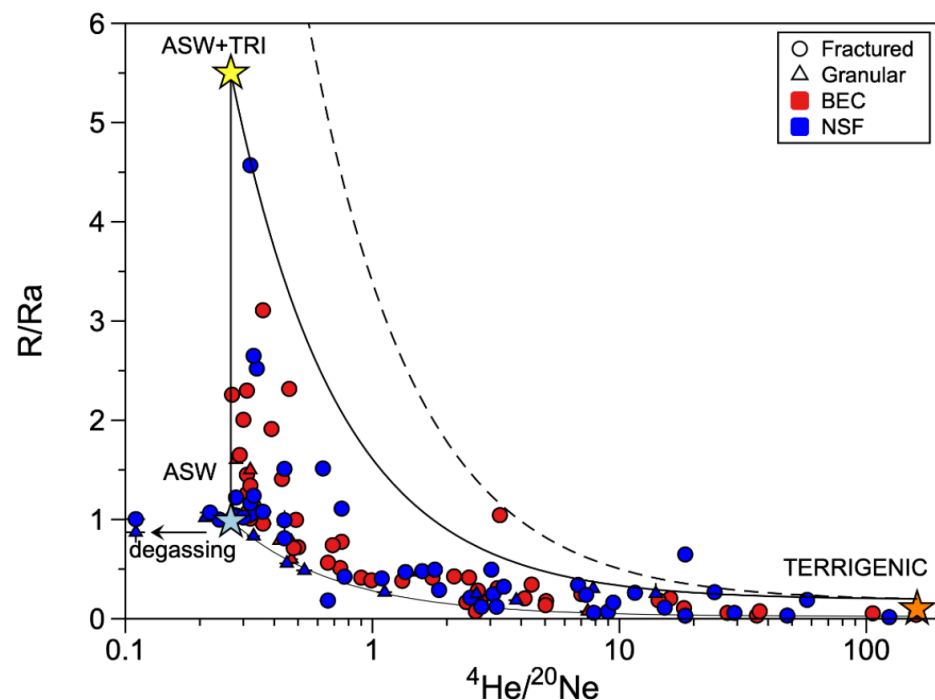


**Figure 2.** Craig’s diagram of  $^4\text{He}/^{20}\text{Ne}$  vs. R/Ra with the three identified endmembers. Plain and dashed lines represent mixing hyperbolas (see text for details).

In the groundwater from aquifers located in stable cratons, it is expected that data will follow mixing between at least two sources: the atmosphere (ASW component) which represents modern meteoric water infiltrating the recharge areas. This component is expected to have a  $^4\text{He}$  and  $^{20}\text{Ne}$  ASW composition ( $^4\text{He}/^{20}\text{Ne}$  of 0.254 at  $10^\circ\text{C}$ ; [50]) and an atmospheric R/Ra close to 1 [52] (Figure 2). The second source is the continental crust

( $^4\text{He}/^{20}\text{Ne} \geq 160$  and  $R/R_a$  of 0.01–0.2; Figure 2) and represents the older groundwater having accumulated radiogenic  $^4\text{He}$  from the surrounding rocks, where it is produced by the decay of U and Th [11]. In the case of the St. Lawrence Lowlands, there is a third source of helium which is meteoric water having dissolved at the recharge tritium from the fallout of the atomic bomb test of the 1950–1960s' period and having accumulated tritiogenic  $^3\text{He}$  produced by the decay of  $^3\text{H}$  (ASW+TRI; Figure 2). This surface water is characterized by an ASW  $^4\text{He}/^{20}\text{Ne}$  ratios of 0.254, but an  $R/R_a$  higher than the atmospheric value caused by the addition of tritiogenic  $^3\text{He}$ . In our studied area, the amount of tritiogenic  $^3\text{He}$  corresponds to the complete decay of 120 TU [27,28], which is significantly higher than the present background value of ca. 10–20 TU, but significantly lower than the tritium-bomb peak in 1962–1965 of 1000–6000 TU [53]. Following the  $^3\text{H}$  decay curve measured in the IAEA station at Ottawa (Ontario) [53], these tritium values were reached between approximately 1961 and 1972, indicating that the tritiated waters recharged the basin between 38 and 51 years ago (with 2010–2013 being the sampling years for this study).

The helium in most of the samples can be accounted for by the mixing of these three sources: (1) meteoric water containing ASW He and Ne and an atmospheric  $R/R_a = 1$ ; (2) sub-modern water having accumulated tritiogenic  $^3\text{He}$  where the complete decay of 120TU corresponds to  $2.99 \times 10^{-13} \text{ cm}^3\text{STP/g}$  of  $^3\text{He}$  ( $1 \text{ TU} = 2.49 \times 10^{-15} \text{ }^3\text{He}$  in  $\text{cm}^3\text{STP/g}$ ) resulting in a  $R/R_a$  of 5.66 (Figure 2); (3) old groundwater enriched in radiogenic  $^4\text{He}$  ( $R/R_a = 0.015$ ) produced in aquifer rocks and containing a small mantle He component corresponding to a fossil signal related to the Cretaceous magmatism of the nearby Montereian Hills ( $R/R_a \geq 0.25$ ; [8,28,54]).

Two samples (piezometer BEC-R4 in Bécancour and well NSF244 in Nicolet-Lower Saint François) plot outside of the traced mixing line between the tritiogenic He and the terrigenous He endmembers (Figure 2). They likely indicate the presence of even higher tritium in the hydrogeological system. It is now known that in the western part of the studied region, (the Vadreuil-Soulanges watershed) there are tritiated waters with initial estimated values of more than 285TU [54]; thus, it is expected that the groundwater will display higher  $R/R_a$  values than those measured up to the present in our studied area. The dashed area plotted in Figure 2 represents the mixing with an endmember having a  $R/R_a$  of 12.2 resulting from the total decay of 285TU of  $^3\text{H}$ . A few samples show  $^4\text{He}/^{20}\text{Ne}$  ratios down to 0.11, smaller than that expected at ASW conditions and corresponding to degassed samples (likely having occurred during sampling), as the solubility of He in water is lower than that of Ne (see also Figure 6) [50].

### 3.2. Helium Isotopic Spatial Distribution and Recharge Confinement Conditions

The identified sources of the helium (Figure 2) indicate the presence of three water bodies: modern meteoric water recently infiltrated; sub-modern water infiltrated in the last 70–80 years and containing anthropogenic tritium; and old groundwater accumulating radiogenic  $^4\text{He}$  produced in the aquifer's rocks or below. If the downward movement of the water in the fractured basal aquifer would behave as a "piston flow"—an unlikely condition in a fractured regional-scale aquifer—it would expect to observe an isotopic helium gradient from the recharge, located south-east in the Appalachians, down to the north-west plain, close to the St-Laurent River. This isotopic gradient would appear as a progressive decrease in the  $^3\text{He}/^4\text{He}$  values, from atmospheric  $R/R_a = 1$  or higher (due to the addition of tritiogenic  $^3\text{He}$ ) at the recharge to lower crustal  $R/R_a$  ratios (0.01–0.1) in the plain.

Figure 3a is the interpolated (kriged)  $R/R_a$  map for the fractured bedrock aquifer, produced using Surfer software (v15.4.354). A few samples from the uppermost Quaternary granular aquifer were excluded as these would create artifact anomalies, due to their very shallow nature and dominated  $R/R_a$  atmospheric signatures, which do not reflect the isotopic signature of the deepest water body.

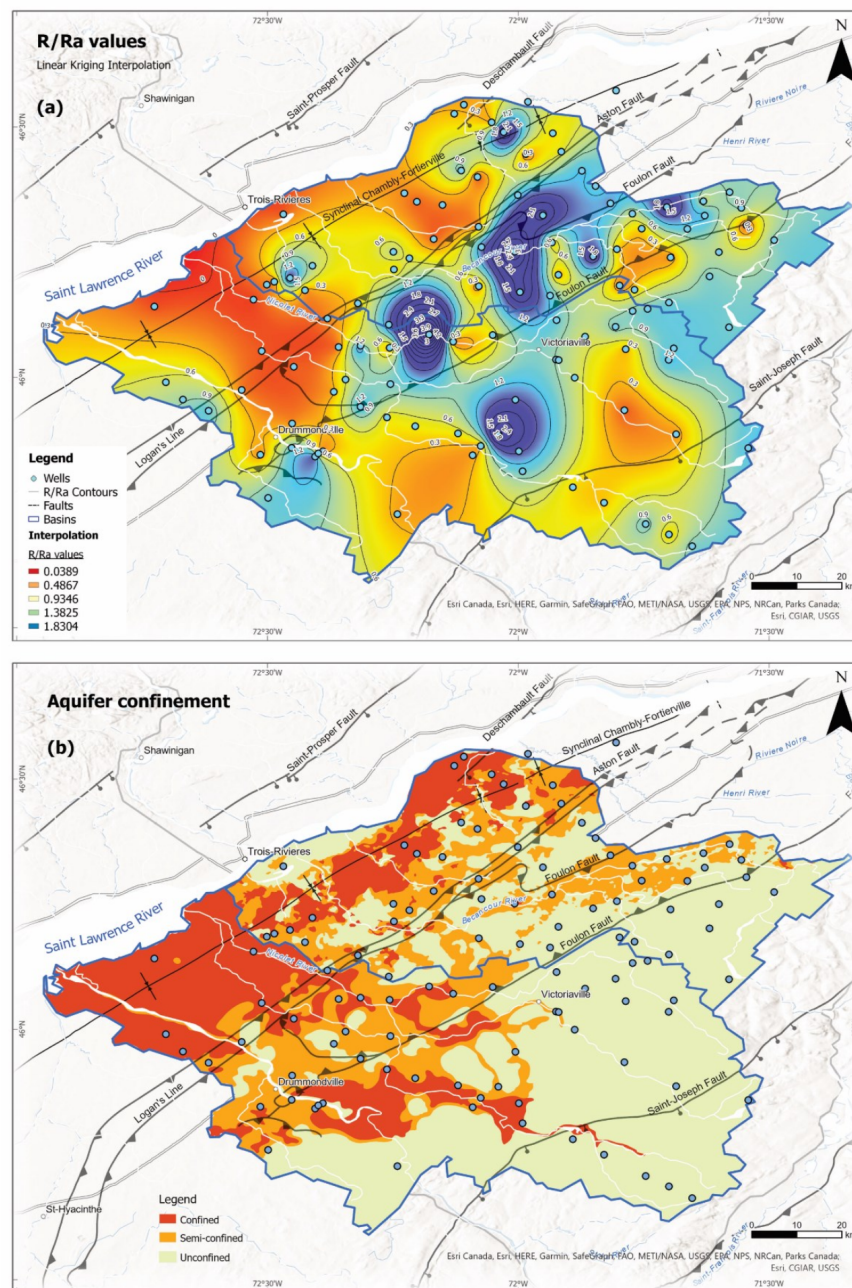


**Figure 3.** (a) Interpolated (kriged) R/Ra map for the fractured bedrock aquifer (unpublished); and (b) Aquifer confinement map (redrawn and adapted with permission from [24,25]).

The original grid size of the map was 2000 rows by 2000 columns, with 4M nodes. The overall mean and median values of R/Ra are 0.645 and 0.751, respectively. The variance and standard deviation of the kriging interpolation are 0.577 and 0.759, respectively. In Figure 3a, the red indicates a dominant radiogenic  $^4\text{He}$  source, i.e., older groundwater, the light yellow and light green indicate a dominant atmospheric helium source (i.e., modern meteoric water), and the blue indicates the occurrence of tritiogenic helium (i.e., sub-modern meteoric water).

Figure 3a highlights the lack of a strong helium isotopic gradient with a SE–NW direction, although most of the radiogenic R/Ra values are found on the plain, closer to the St. Laurent River where the most confining conditions are found (Figure 3b). The gradient is disrupted by the presence of mid-distance spots where tritiogenic helium occurs, indicating sub-modern water (the blue spots in Figure 3a). Interestingly, a comparison of

this distribution with the aquifer confinement conditions (Figure 3b) shows that the green, blue and red areas correspond roughly to the unconfined, semi-confined and confined zones of the regional bedrock fractured aquifer, as estimated by [24,25]. The match is not perfect for two reasons. First, the kriging is necessarily approximate because of the low-medium spatial distribution of the sampled wells where the  $^3\text{He}/^4\text{He}$  ratio was measured (121 points covering 7500 km<sup>2</sup>). Second, the confinement of the aquifer has been determined using a 3D model of the architecture of the impermeable Quaternary sediments, tillites and clays. The confinement levels of the aquifer depend on the thickness of those impermeable rock units (tillites and clays) and if several of them are present, only the thickest is considered and not the sum of all of them. Then, the results are interpolated on a 250 × 250 m grid. The aquifers are considered “confined” if covered by more than 3 m of clay or 5 m of tillite; “semi-confined” if covered by 1 to 3 m of clay and 3 to 5 m of tillite; and “unconfined” if covered by less than 1 m of clay or less than 3 m of tillite [24,25]. Therefore, the confinement condition map’s precision depends on the resolution of the geological mapping in the area and the chosen “qualitative” conditions of impermeability.

There is one elongated area located in a region closer to the recharge area, SE of Victoriaville town (Figure 3b) where, although unconfined aquifers are expected, relatively high radiogenic  $^4\text{He}$  concentrations of  $4.16 \times 10^{-7}$  cm<sup>3</sup>STP/g (and a R/Ra value of 0.211) are observed in sample NSF165, which has an evolved Na-HCO<sub>3</sub> chemistry. These parameters suggest long residence times and confined conditions at depth. However, the two closer wells display nearly ASW  $^4\text{He}$  contents and Ca-HCO<sub>3</sub> chemistry, characteristic of the recharge area. Such localized anomalies suggest that the additional kriging filtering is needed and highlight the limitations of this method when data are scarce.

To determine “quantitatively” the possible relation between the aquifer confinement conditions of the fractured bedrock aquifer and the  $^3\text{He}/^4\text{He}$  ratios, we superimposed the two maps and extrapolated the aquifer confinement conditions for each of the sampling points where helium was determined (Table S1, Supplementary Materials). A simple Whisker plot (Figure S1, Supplementary Materials) shows that the median R/Ra values for the three classes of confinement (unconfined, semiconfined and confined) differ: 0.996; 0.399; and 0.172, respectively. This indicates a progressive increase in the radiogenic  $^4\text{He}$  in the groundwater, as the aquifer becomes progressively confined. Interestingly, most outliers with the highest tritiogenic R/Ra up to 4.57 fall also in the category of the semi-confined aquifers (Figure S1, Supplementary Materials). To determine if the differences in the calculated median values for each category are statistically significant (i.e., the samples do not belong to the same distribution), a Kruskal–Wallis test was carried out. This non-parametric test, performed using R, can be applied when the data do not follow a normal distribution, as is the case with our dataset. The most important result of this test is the so-called *p*-value (which is equal to 0.02288 for our test). If the *p*-value is lower than the significance level  $\alpha$ , which is usually taken as 0.05 (i.e., there is a 5% risk of concluding that a difference between median values exists when there is no actual difference) then we can conclude that the differences in the calculated median values are statistically significant.

It can be questioned if other parameters, such as faulting (see also the isolated anomalies along the downmost branch of the Foulon Fault, in the eastern sector of the Bécancour watershed; Figure 3a), could locally influence the spatial distribution of helium in the basin. The previous work on the hydrogeology of the region did not find any evidence of tectonic control on the hydrodynamics of the basin [24,25,35]. However, a study of helium and methane in the groundwater from the same region, completed by Moritz et al. [55], showed a rough possible relation between the concentration of  $^4\text{He}$  and the distance to the main tectonic accidents. A localized tectonic control of the release of radiogenic helium in the groundwater is thus plausible but requires further investigation.

This comparison highlights the usefulness of producing detailed kriging maps where confinement conditions that are at a depth, independent from the surface geology, can be correctly evaluated when the R/Ra ratios are available for a statistically significant numbers of the wells for a given area.

### 3.3. Helium Isotopic Signature and Groundwater Chemistry

The progressive decrease in the R/Ra ratios (Figure 2) is related to the progressive addition of radiogenic  $^4\text{He}$  (see also below Section 3.4 and Figure 5). If accumulation of radiogenic  $^4\text{He}$  results from in situ production in the aquifer itself and helium progressively released from the reservoir rock into the groundwater, a relationship may be present with the evolving chemistry of water over time and its dissolved solids. Yet, it is uncommon to observe a well-defined relationship between the dissolved ions and helium, except for a few examples (e.g., [6,56]). This may be the result of two processes. The first one is related to the kinetics of transfer of He and dissolved solids from the rock to groundwater. The concentrations of the dissolved solids depend mainly on the dissolution rate of the rock. Helium, as a gas trapped in the rock's crystalline structure, can be transferred into the groundwater, either during rock dissolution/weathering, or by diffusion or  $\alpha$ -recoil [11]. To be an efficient transfer process, diffusion and  $\alpha$ -recoil require that helium is close to the surface grains, so that any mechanism that can increase the specific surface of the rock exposed to groundwater will favor the release of helium into the fluid phase. This can be weathering [11], or tectonically induced fracturing [57]. In glaciated areas, such as the studied area in the Late Quaternary in this study, rock fracturing during the deglaciation processes can also favor the episodic release of important amounts of radiogenic  $^4\text{He}$  into water [58]. Therefore, different kinetics can control the release of dissolved ions and helium, decoupling them. The second process responsible for a decoupling are sources of helium external to the aquifer. There is abundant literature regarding an excess of radiogenic  $^4\text{He}$  in groundwater, which point to a groundwater residence time several orders of magnitude higher than those independently obtained with other water chronometers, such as  $^{14}\text{C}$  (e.g., [5,27,59–62]). This suggests the addition of a continental upward helium flux into the aquifers (e.g., [63–65]). If this continental flux is not spatially constant, this may induce further decoupling between  $^4\text{He}$  and the dissolved solids.

In Figure 4, the  $^4\text{He}/^3\text{He}$  ratios are plotted against the TDS (Total Dissolved Solids), calculated as the sum of the major cations and anions dissolved in water.

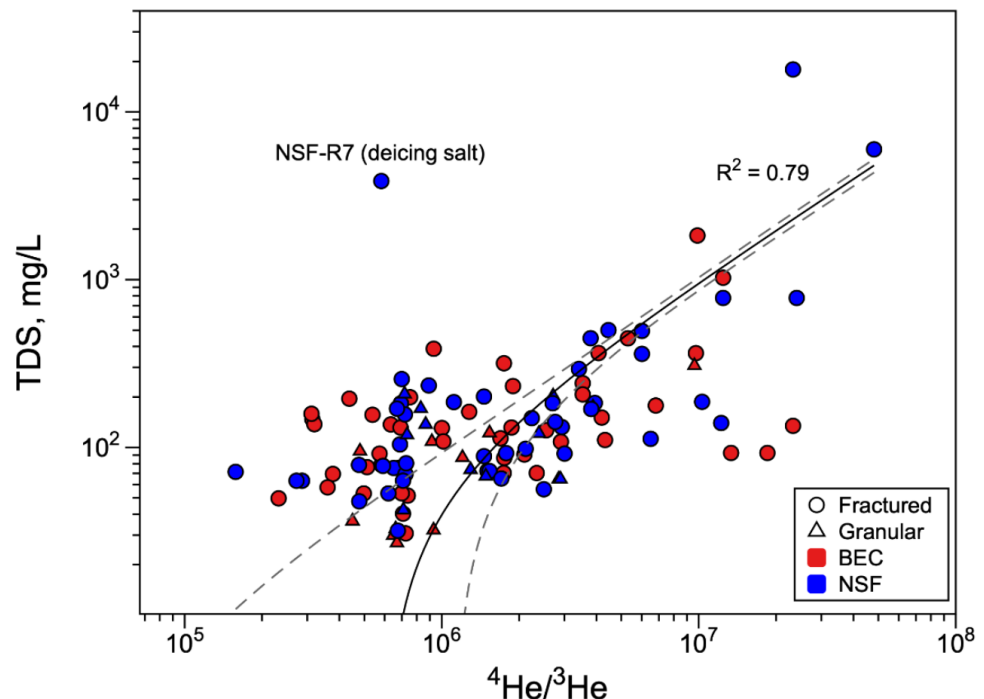


**Figure 4.** Total Dissolved Solids as a function of  $^4\text{He}/^3\text{He}$  ratios in groundwater samples. Linear regression (plain line) computed excluding  $1.5\sigma$  outliers (essentially, sample NSF-R7) is reported with the goodness-of-fit measure  $R^2$  parameter. Dashed lines represent the 95% confidence interval bounds.

It is possible to see a rough positive trend (not linear, shown as a log–log plot) which suggests that the increase in radiogenic  $^4\text{He}$  addition is accompanied by a release of solids from the aquifer rocks. The linear regression through the datapoint gives a  $R^2 = 0.79$  (Figure 4). An outlier is sample NSF-R7, previously identified by [28] as contaminated by road deicing salt. Interestingly, the slope of this trend is about 2/3 in a log–log scale. This means that the helium increased more rapidly than the chemical constituents, maybe also suggesting the addition of a helium source external to the aquifer, as a crustal helium flux [65].

If this trend is meaningful, other uncommon relationships are expected to be present with specific cations or anions. While no other obvious relationships are readily observed, the same does not hold true when basic statistics are applied, and data are grouped by the chemical groundwater families identified in the area [39]. The latter highlight the presence of apparent trends with respect of water chemistry evolution, helium isotopes and residence times (Figure 5).

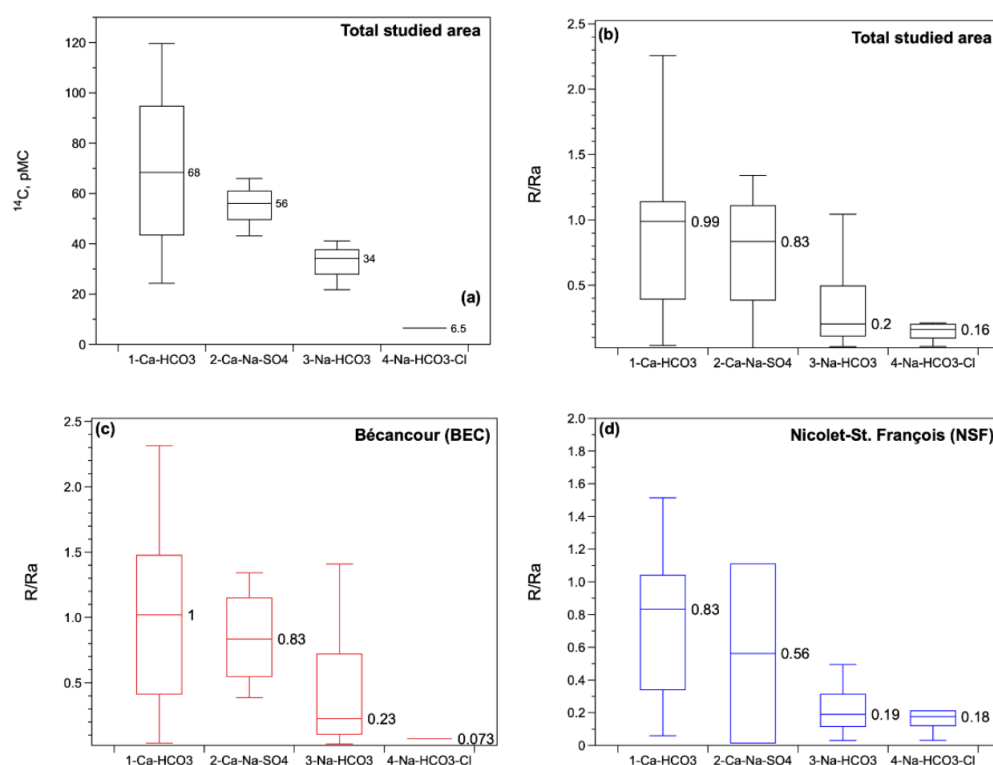


**Figure 5.** (a)  $^{14}\text{C}$  activities in pMC; (b)  $R/Ra$  values measured for the entire studied area, and  $R/Ra$  values for samples from (c) the Bécancour watershed and (d) the Nicolet—St. François watershed. All data refer to the fractured regional aquifer.

The different categories used for the Whisker plots are the chemical families of the waters which correspond to the progressive chemical evolution of groundwater caused by prolonged water–rock interactions over time, as identified by [39,40]. The numerals next to each boxplot are the median values calculated for each specific category. Although qualitative, this first-order statistical approach is useful to smooth variability and to show that with the progressive water ageing (represented by the progressive decrease in the  $^{14}\text{C}$  activity), progressive accumulation of radiogenic  $^4\text{He}$ , as well as a modification of the water chemistry, takes place. This latter results in chemical changes from bicarbonate in the recharge area to sodium-carbonate in the discharge areas by ionic exchange, and finally dissolution of the NaCl trapped in the Holocene clays deposited by the Champlain Sea (Figure 5) [41].

### 3.4. Helium as a Water Chronometer

The results shown in Figures 4 and 5 suggest that radiogenic  $^4\text{He}$  accumulation is derived mainly from in situ production in the aquifer, with the possible addition of a crustal flux. In Figure 6, the R/Ra values plotted against the inverse of  $^4\text{He}$  concentrations show an expected positive correlation, pointing to an accumulation of radiogenic  $^4\text{He}$  over time, with resulting decrease in the  $^3\text{He}/^4\text{He}$  ratio. Only two of the samples do not follow this general trend because they were degassed, creating a deficit in He compared with the ASW minimal value expected at the recharge.

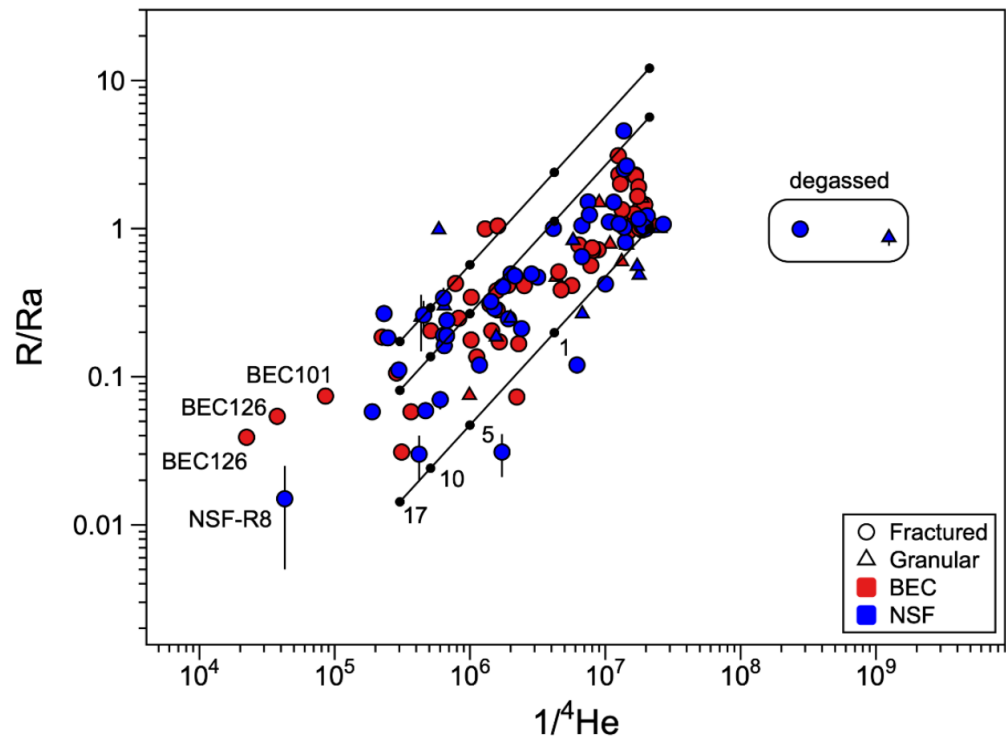


**Figure 6.** R/Ra values as a function of the inverse of the  $^4\text{He}$  content. Numerals next to the black dots are helium accumulation ages in K yrs (kiloyears).

The rate of accumulation of radiogenic  $^4\text{He}$  ( $[^4\text{He}]_{\text{acc}}$ ; Equation (1) in  $\text{cm}^3\text{STP/g yr}$ ) can be modeled assuming, for example, in situ production of radiogenic helium through the equation (e.g., [12]):

$$[^4\text{He}]_{\text{acc}} = \rho \times \Lambda \times P_{4\text{He}} \times \frac{1 - \phi}{\phi} \tag{1}$$

where  $\rho$  is the density of the basal aquifer rocks ( $2720 \text{ kg/m}^3$ ; [27]);  $\Lambda$  is the fraction of He produced in the rock that is released into the water phase—this is assumed to be unity [66];  $P_{4\text{He}}$  is the production rate of radiogenic  $^4\text{He}$  from U and Th in rocks;  $\phi$  is the effective porosity. Multiplying the  $[^4\text{He}]_{\text{acc}}$  for  $t$ , the residence time of water in the aquifer, the total amount of excess  $^4\text{He}$  to be added to the  $^4\text{He}$  ASW content (here assumed to be  $4.75 \times 10^{-8} \text{ cm}^3\text{STP/g}$  at  $10^\circ\text{C}$ ) can be estimated. Three curves were calculated, assuming the best conditions for a high radiogenic  $^4\text{He}$  in situ production, i.e., the maximum  $P_{4\text{He}}$  in the basal aquifer rocks of  $7.23 \times 10^{-10} \text{ cm}^3\text{STP/g}_{\text{rock}} \text{ yr}$  based on the highest measured U and Th contents of 3 and 13 ppm in the fractured aquifer [27] and a minimum porosity measured for these rocks of 1% [67], a value close to the 1.5% we assumed for the same bedrock fractured aquifer during the MODFLOW simulation of the groundwater circulation in the same region as studied here [37]. The three curves reported in Figure 6 represent the evolution of the  $^3\text{He}/^4\text{He}$  ratio by progressive addition of radiogenic, in situ

produced  $^4\text{He}$  (nucleogenic  $^3\text{He}$  production from  $^6\text{Li}$  is negligible and, thus, is not taken into consideration in the calculation; [8,54]) with time. The numerals indicate the residence time in ka, with the maximum of 17.05 ka which corresponds to the highest  $^{14}\text{C}$  corrected ages obtained in the studied area (Table S1, Supplementary Materials). Three departing points were selected: pure ASW conditions corresponding to  $^4\text{He} = 4.75 \times 10^{-8} \text{ cm}^3\text{STP/g}$  and  $R/\text{Ra} = 1$ ; a tritiogenic water containing 120TU which corresponds to a  $R/\text{Ra} = 5.66$ ; a second tritiogenic water containing 285TU which corresponds to a  $R/\text{Ra} = 12.1$ , the maximum value calculated by [54] in the St. Lawrence Lowlands' groundwaters. Except for the samples BEC126, BEC101 and NSF-R8, all of the data can be accounted for by the in situ production of helium in the low porosity zones of the fractured basal aquifer. The  $^{14}\text{C}$  age of NSF-R8 was not determined, but that of BEC126 is 9200 a, and that of BEC101 of 7900 a, based on the Fontes and Garnier [47] method (Table S1, Supplementary Materials). If a porosity of 0.1% is assumed, then the  $^{14}\text{C}$  corrected ages and U-Th/ $^4\text{He}$  in situ ages would be concordant, but such low porosities are not coherent with those measured by [67] of 1–5% and measured hydraulic conductivities [24,25]. Based on the relationship between porosity and hydraulic conductivity of Kozeny–Carman [68], and using typical specific surface values of carbonates and carbonate-shales rocks [69] as those of the fractured basal aquifer, for porosities of 0.1% we would obtain hydraulic conductivities as low as  $10^{-15} \text{ m/s}$  against the minimum measured values of  $10^{-9} \text{ m/s}$  [24]. Further, the BEC126 sample is dramatically poorly mineralized, which would suggest that interaction with rocks were minimal.

The relation between TDS and  $R/\text{Ra}$  values suggest that helium is released faster than dissolved solids, which could be related either to different mechanisms of release of He and the dissolved load and/or to the addition of a basal crustal flux. Calibrating the  $^{14}\text{C}$  ages against the calculated (U-Th)/ $^4\text{He}$  ages (using equation 1), the authors of [27] judged the presence of a variable crustal flux of  $9.0\text{--}59 \times 10^{-8} \text{ cm}^3 \text{ STP/cm}^2 \text{ yr}$ . This flux is 32 to 583 times lower than the helium flux calculated from the Canadian Precambrian Shield ( $5.83 \times 10^{-6} \text{ cm}^3 \text{ STP/cm}^2 \text{ yr}$ ; [65]), suggesting that the local aquifer rocks are the dominant source of He.

Another explanation of the anomalously high radiogenic  $^4\text{He}$  in BEC101 and BEC126 comes from the work of Méjean et al. [70]. They showed that those groundwater samples are enriched in both radiogenic  $^4\text{He}$  and  $^{234}\text{U}$ , another isotope of the U–Th decay chain. The  $^{234}\text{U}$  resides on the damaged crystal lattice sites or on grain surfaces, while only the  $^4\text{He}$  close to the grain surface is the one released promptly into the water phase by  $\alpha$ -recoil or diffusion. Méjean et al. [54] proposed that the loading and unloading caused by the Laurentide Ice Sheet migration might have induced large-scale near-surface tectonic stresses, inducing fracturing of the aquifer. Exposed new fractures of the basal aquifer would have favored the release of large amounts of radiogenic  $^4\text{He}$  from rocks into water pockets, as those sampled by the BEC126 and BEC101 wells. The model proposed by Méjean et al. [54] suggests that the past recharge of aquifers in the region was dominantly ice glacier-driven. Interestingly, calculated noble gas recharge paleotemperatures for BEC126 are close to  $0^\circ\text{C}$ , suggesting the presence of poorly mineralized glacial or postglacial water, possibly recharging the aquifer during the last phases of deglaciation of the region (see the next section).

### 3.5. Noble Gas Paleotemperatures and Recharge Conditions during the Holocene

Figure 7 reports the calculated NGT vs. the corrected  $^{14}\text{C}$  ages. The noble Gas temperatures are not only important as an independent continental climatic proxy, but they can also provide valuable information on how the aquifer's recharge reacted during the glacial and interglacial periods in the past, providing a window into the future.

An increase in the NGTs is observed from values close to  $0^\circ\text{C}$  at around 10,000 years, at the end of the deglaciation in the center of Québec [36] to values of  $6\text{--}8^\circ\text{C}$  at around 5–7 ka, which corresponds to the Mid Holocene Climate Optimum (MHO) in the region. This warmer temperature anomaly has been also recorded in pollen in Lanoraie peats

located on the north shore of the St. Laurent River, NW of the NSF watershed [71] (the dark green plain line in Figure 7) and from lake sediments from SE Québec on the Appalachians (the light green dashed line in Figure 7) [72]). The first site represents the climatic conditions of the St. Lawrence Lowlands plain, the second site of the Appalachian recharge (Figure 1).

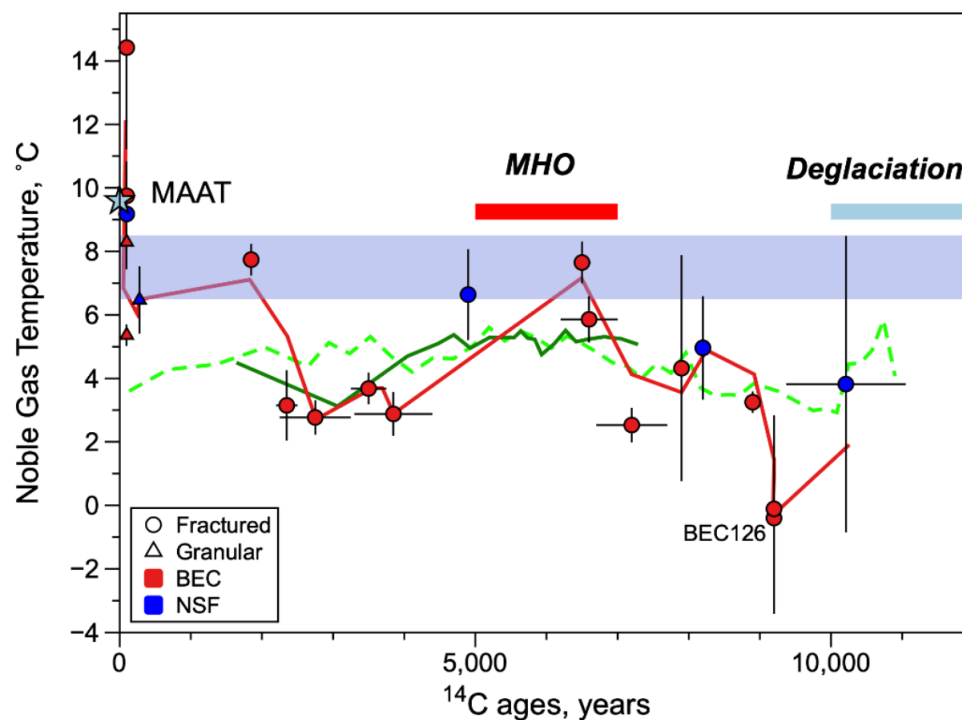


**Figure 7.** Noble gas temperatures as a function of  $^{14}\text{C}$  ages in groundwater samples. The red line is the moving average. The dark green line and the light green dashed line are temperatures recorded by pollen from peat and lake sediments (see text for details). Blue star labeled MAAT = Mean Annual Ambient Temperature; MHO = Mid-Holocene Climate Optimum. The blue band represents the average recharge temperatures during the spring and autumn recharge periods.

Following the MHO, the NGT record shows a cooler (2–3 °C) short period at around 2–4 ka, also recorded in the Lanoraie peat pollen but not visible in the Appalachian sediment records, followed by an NGT increase to warmer temperatures in modern times, similar to those of the present-day recharge. This temperature trend suggests that the recharge was also active in the ice-covered regions [21], despite atmospheric temperatures below the freezing point (Figure 7), as also indicated by the older NGT records obtained from the Michigan Basin Marshall and Saginaw aquifers' groundwater [2], and independent geophysical observations. Temperature-depth profiles obtained from boreholes in Eastern Canada were inverted to determine the ground surface temperature record during and after the last glacial cycle [73]. The inversions yielded ground surface temperatures ranging from −1.4 to 3.0 °C throughout the last glacial cycle. These temperatures, near the pressure melting point of ice, allowed the basal flow and fast flowing ice streams at the base of the Laurentide Ice Sheet [73].

#### 4. Conclusions

The results from this study show that, even in heterogeneous fractured regional-scale aquifers, noble gas and especially helium isotopes measured in groundwater, can be useful to trace the chemical evolution of water and the confinement conditions. A subset of samples for which the noble gas temperatures were estimated also shows, as previously observed in similar post-glacial aquifers of North America, that even in colder, ice-covered periods, groundwater recharge can occur. Most interestingly, the spatial distribution of the  $^3\text{He}/^4\text{He}$  ratios can be used for determining, independently from semi-qualitative

estimations based on surface geology, the confinement conditions along the expected flow path. In the south shore watersheds of the St. Lawrence Lowlands, the spatial distribution of the  $^3\text{He}/^4\text{He}$  ratios measured in the groundwaters roughly follows the confinement patterns, with the most radiogenic  $^4\text{He}$  waters in the deeper confined part of the aquifer, and ASW and tritiogenic  $^3\text{He}$  in the free and semi-confined aquifers, even when the sampling density is very low (121  $^3\text{He}/^4\text{He}$  data on 7500 km<sup>2</sup> of territory). The high-density helium isotopic surveys in smaller areas (to control high analytical costs) could be very useful for deconvoluting the aquifer recharge conditions, for example, in complex hydrogeological situations. If the helium isotopic signature of the groundwater evolves during extended residence time periods, correlations with the total dissolved solids remain elusive, because the transfer rates and processes between chemical load and gases into water are different. Yet, in the studied area, basic statistics show a co-evolution of the chemistry of water and radiogenic  $^4\text{He}$  accumulation with time. This suggests that radiogenic  $^4\text{He}$  in the basin is mainly from local sources, although a small contribution of a crustal basal helium flux could also be at play [27]. Finally, the noble gas temperatures obtained from other noble gas data can be helpful to better delineate the recharge conditions in different climates, particularly in areas of North America which were ice-covered until the Holocene.

In conclusion, this work highlights the importance of studying the spatial distribution of groundwater isotopes/tracers to detect the dynamics of flow and the recharge conditions at watershed or even at basin scale. The limitations for noble gases to cover large aquifers with a statistically significant number of samples are caused by elevated analytical costs and time-spending analyses (e.g., [74]). Yet, a new generation of portable and autonomous mass spectrometric systems [75] for the elemental analyses of noble gases and even for helium isotopic ratios [76], will reduce drastically the costs and time for analyses of noble gases, allowing helium and other inert gases to be used to determine, at a basin scale, the groundwater recharge areas and flow.

**Supplementary Materials:** The following supporting information can be downloaded at: <https://www.mdpi.com/article/10.3390/w14121940/s1>, Table S1: Samples' characteristics, helium data together with  $^{14}\text{C}$  corrected ages and  $^3\text{H}/^3\text{He}$  apparent ages; Table S2: noble gas concentrations together with neon excess ( $\Delta\text{Ne}$ ) and calculated noble gas temperatures (in °C); Figure S1: Whisker plot of R/Ra values vs. aquifer confinement conditions.

**Author Contributions:** Conceptualization, D.L.P.; methodology, D.L.P., M.C.C. and Y.S.; software, M.A.H.-H. and V.H.; validation, D.L.P., M.L., P.M., M.S., M.A.H.-H., S.G., E.R., Y.S., M.C.C. and T.M.; analysis, D.L.P., P.M., M.S., M.A.H.-H. and E.R.; investigation, D.L.P., P.M., M.S. and M.A.H.-H.; resources, D.L.P., M.L., M.C.C., Y.S. and T.M.; data curation, D.L.P., M.S. and P.M.; writing—original draft preparation, D.L.P.; writing—review and editing, D.L.P., M.L., P.M., M.S., M.A.H.-H., S.G., E.R., Y.S., M.C.C., V.H. and T.M.; visualization, D.L.P., P.M. and V.H.; supervision, D.L.P. and M.L.; project administration, S.G.; funding acquisition, D.L.P. and M.L. All authors have read and agreed to the published version of the manuscript.

**Funding:** This research was essentially funded by Ministère du Développement durable, de l'Environnement et de la Lutte contre les changements climatiques, through the Programme d'acquisition de connaissances sur les eaux souterraines—PACES (Groundwater acquisition program) to M.L., Fonds de recherche du Québec-Nature et Technologies through the Projets de recherche orientée en partenariat/Eaux souterraines du Québec project no. 136990 to D.L.P.

**Data Availability Statement:** Data used for this work are reported in Tables S1 and S2. Further data on the sampled wells (chemistry and physical parameters) can be requested directly from DLP or ML.

**Acknowledgments:** This work was carried out as a part of the IAEA Coordinated Research Projects on Use of Long-lived Radionuclides for Dating Very Old Groundwaters (IAEA CRP F33023). We wish to thank the three anonymous reviewers for their thoughtful comments.

**Conflicts of Interest:** The authors declare no conflict of interest.

## References

1. Beyerle, U.; Aeschbach-Hertig, W.; Hofer, M.; Imboden, D.; Baur, H.; Kipfer, R. Infiltration of river water to a shallow aquifer investigated with  $^3\text{H}/^3\text{He}$ , noble gases and CFCs. *J. Hydrol.* **1999**, *220*, 169–185. [[CrossRef](#)]
2. Hall, C.M.; Castro, M.C.; Lohmann, K.C.; Ma, L. Noble gases and stable isotopes in a shallow aquifer in southern Michigan: Implications for noble gas paleotemperature reconstructions for cool climates. *Geophys. Res. Lett.* **2005**, *32*, L18404. [[CrossRef](#)]
3. Wen, T.; Castro, M.C.; Hall, C.M.; Pinti, D.L.; Lohmann, K.C. Constraining groundwater flow in the glacial drift and saginaw aquifers in the Michigan Basin through helium concentrations and isotopic ratios. *Geofluids* **2016**, *16*, 3–25. [[CrossRef](#)]
4. Medici, G.; Engdahl, N.B.; Langman, J.B. A Basin-Scale Groundwater Flow Model of the Columbia Plateau Regional Aquifer System in the Palouse (USA): Insights for Aquifer Vulnerability Assessment. *Int. J. Environ. Res.* **2021**, *15*, 299–312. [[CrossRef](#)]
5. Duckett, K.A.; Langman, J.B.; Bush, J.H.; Brooks, E.S.; Dunlap, P.; Stanley, J.R. Noble gases, dead carbon, and reinterpretation of groundwater ages and travel time in local aquifers of the Columbia River Basalt Group. *J. Hydrol.* **2020**, *581*, 124400. [[CrossRef](#)]
6. Castro, M.C.; Jambon, A.; De Marsily, G.; Schlosser, P. Noble gases as natural tracers of water circulation in the Paris Basin: 1. Measurements and discussion of their origin and mechanisms of vertical transport in the basin. *Water Resour. Res.* **1998**, *34*, 2443–2466. [[CrossRef](#)]
7. Ma, L.; Castro, M.C.; Hall, C.M. Crustal noble gases in deep brines as natural tracers of vertical transport processes in the Michigan Basin. *Geochem. Geophys. Geosyst.* **2009**, *10*, Q06001. [[CrossRef](#)]
8. Pinti, D.L.; Béland-Otis, C.; Tremblay, A.; Castro, M.C.; Hall, C.M.; Marcil, J.-S.; Lavoie, J.-Y.; Lapointe, R. Fossil brines preserved in the St-Lawrence Lowlands, Québec, Canada as revealed by their chemistry and noble gas isotopes. *Geochim. Cosmochim. Acta* **2011**, *75*, 4228–4243. [[CrossRef](#)]
9. Aggarwal, P.K.; Matsumoto, T.; Sturchio, N.; Chang, H.K.; Gastmans, D.; Araguas-Araguas, L.J.; Jiang, W.; Lu, Z.-T.; Mueller, P.; Yokochi, R.; et al. Continental degassing of  $^4\text{He}$  by surficial discharge of deep groundwater. *Nat. Geosci.* **2014**, *8*, 35–39. [[CrossRef](#)]
10. Tolstikhin, N.I.; Kamensky, I.L. On the Possibility of Groundwater Dating by the Tritium-Helium-3 Method. *Geokhimiya* **1969**, *8*, 1027–1029.
11. Torgersen, T. Controls on pore-fluid concentration of  $^4\text{He}$  and  $^{222}\text{Rn}$  and the calculation of  $^4\text{He}/^{222}\text{Rn}$  ages. *J. Geochem. Explor.* **1980**, *13*, 57–75. [[CrossRef](#)]
12. Kulongoski, T.J.; Hilton, D.R. Applications of Groundwater Helium. In *Handbook of Environmental Isotope Geochemistry*; Springer Isotope Handbook: Reston, VA, USA, 2011; Volume 1, pp. 285–304.
13. Holland, G.P.; Lollar, B.S.; Li, L.; Lacrampe-Couloume, G.; Slater, G.F.; Ballentine, C. Deep fracture fluids isolated in the crust since the Precambrian era. *Nature* **2013**, *497*, 357–360. [[CrossRef](#)]
14. Heard, A.W.; Warr, O.; Borgonie, G.; Linage, B.; Kuloyo, O.; Fellowes, J.W.; Magnabosco, C.; Lau, M.C.Y.; Erasmus, M.; Cason, E.D.; et al. South African Crustal Fracture Fluids Preserve Paleometeoric Water Signatures for up to Tens of Millions of Years. *Chem. Geol.* **2018**, *493*, 379–395. [[CrossRef](#)]
15. Mazar, E. Paleotemperatures and other hydrological parameters deduced from noble gases dissolved in groundwaters; Jordan Rift Valley, Israel. *Geochim. Cosmochim. Acta* **1972**, *36*, 1321–1336. [[CrossRef](#)]
16. Stute, M.; Schlosser, P. Principles and Applications of the Noble Gas Paleothermometer. In *Climate Change in Continental Isotopic Records*; Swart, P.K., Lohmann, K.C., McKenzie, J., Savin, S., Eds.; AGU: Washington, DC, USA, 1993; pp. 89–100.
17. Aeschbach-Hertig, W.; Peeters, F.; Beyerle, U.; Kipfer, R. Palaeotemperature reconstruction from noble gases in ground water taking into account equilibration with entrapped air. *Nature* **2000**, *405*, 1040–1044. [[CrossRef](#)]
18. Castro, M.C.; Warrier, R.B.; Hall, C.M.; Lohmann, K.C. A late Pleistocene-Mid-Holocene noble gas and stable isotope climate and subglacial record in southern Michigan. *Geophys. Res. Lett.* **2012**, *39*, L19709. [[CrossRef](#)]
19. Seltzer, A.M.; Ng, J.; Aeschbach, W.; Kipfer, R.; Kulongoski, J.T.; Severinghaus, J.P.; Stute, M. Widespread six degrees Celsius cooling on land during the Last Glacial Maximum. *Nature* **2021**, *593*, 228–232. [[CrossRef](#)]
20. Beyerle, U.; Purtschert, R.; Aeschbach-Hertig, W.; Imboden, D.M.; Loosli, H.H.; Wieler, R.; Kipfer, R. Climate and Groundwater Recharge during the Last Glaciation in an Ice-Covered Region. *Science* **1998**, *282*, 731–734. [[CrossRef](#)]
21. Piotrowski, J.A. Groundwater under Ice Sheets and Glaciers. *Glacier Sci. Environ. Chang.* **2006**, *50*–60. [[CrossRef](#)]
22. Lemieux, J.-M.; Sudicky, E.A.; Peltier, W.R.; Tarasov, L. Dynamics of groundwater recharge and seepage over the Canadian landscape during the Wisconsinian glaciation. *J. Geophys. Res. Earth Surf.* **2008**, *113*. [[CrossRef](#)]
23. Carrier, A.M.; Lefebvre, R.; Rivard, C.; Parent, M.; Ballard, J.-M.; Benoit, N.; Vigneault, H.; Beaudry, C.; Malet, X.; Laurencelle, M.; et al. *Portrait des Ressources en Eau Souterraine en Montérégie Est*; Institut National de la Recherche Scientifique (INRS-Eau): Montréal, QC, Canada, 2013.
24. Larocque, M.; Gagné, S.; Tremblay, L.; Meyzonat, G. *Projet de Connaissance des Eaux Souterraines du Bassin Versant de la Rivière BéCancour et de la Mrc de BéCancour*; Université du Québec à Montréal: Montréal, QC, Canada, 2013; p. 219.
25. Larocque, M.; Gagné, S.; Barnette, D.; Meyzonat, G.; Graveline, M.H.; Ouellet, M.A. *Projet de Connaissance des Eaux Souterraines de la Zone Nicolet et de la Partie Basse de la Zone Saint-François*; Université du Québec à Montréal: Montréal, QC, Canada, 2015; p. 241.
26. Beaudry, C.; Lefebvre, R.; Rivard, C.; Cloutier, V. Conceptual model of regional groundwater flow based on hydrogeochemistry (Montérégie Est, Québec, Canada). *Can. Water Resour. J.* **2018**, *43*, 152–172. [[CrossRef](#)]
27. Vautour, G.; Pinti, D.L.; Méjean, P.; Saby, M.; Meyzonat, G.; Larocque, M.; Castro, M.C.; Hall, C.M.; Boucher, C.; Roulleau, E.; et al.  $^3\text{H}/^3\text{He}$ ,  $^{14}\text{C}$  and (U-Th)/He groundwater ages in the St. Lawrence Lowlands, Quebec, Eastern Canada. *Chem. Geol.* **2015**, *413*, 94–106. [[CrossRef](#)]

28. Saby, M.; Larocque, M.; Pinti, D.L.; Barbecot, F.; Sano, Y.; Castro, M.C. Linking groundwater quality to residence times and regional geology in the St. Lawrence Lowlands, southern Quebec, Canada. *Appl. Geochem.* **2016**, *65*, 1–13. [[CrossRef](#)]
29. Globensky, Y. *Géologie des Basses Terres Du Saint-Laurent*; Ministère des Richesses Naturelles du Québec: Québec, QC, Canada, 1987; p. 63.
30. Tremblay, A.; Pinet, N. Late Neoproterozoic to Permian tectonic evolution of the Quebec Appalachians, Canada. *Earth-Sci. Rev.* **2016**, *160*, 131–170. [[CrossRef](#)]
31. Lavoie, D.; Rivard, C.; Lefebvre, R.; Séjourné, S.; Thériault, R.; Duchesne, M.; Ahad, J.; Wang, B.; Benoit, N.; Lamontagne, C. The Utica Shale and gas play in southern Quebec: Geological and hydrogeological syntheses and methodological approaches to groundwater risk evaluation. *Int. J. Coal Geol.* **2014**, *126*, 77–91. [[CrossRef](#)]
32. Perrot, M.; Tremblay, A. Structural characterization of late Silurian normal faults in the Quebec Appalachians: Implications for sedimentary basin formation and Laurentian margin exhumation during the Salinic orogeny. *J. Struct. Geol.* **2021**, *150*, 104397. [[CrossRef](#)]
33. Globensky, Y.; et collaborateurs. *Lexique Stratigraphique Canadien: Région des Appalaches, des Basses-Terres du Saint-Laurent et des Îles de la Madeleine*; Ministère de l'énergie et des Ressources: Québec, QC, Canada, 1993; p. 327.
34. Lamothe, M. A New Framework for the Pleistocene Stratigraphy of the Central St. Lawrence Lowland, Southern Québec. *Geogr. Phys. Quat.* **1989**, *43*, 119–129. [[CrossRef](#)]
35. Malgrange, J.; Gleeson, T. Shallow, old, and hydrologically insignificant fault zones in the Appalachian orogen. *J. Geophys. Res. Solid Earth* **2014**, *119*, 346–359. [[CrossRef](#)]
36. Occhietti, S.; Richard, P.J. Effet réservoir sur les âges  $^{14}\text{C}$  de la Mer de Champlain à la transition Pléistocène-Holocène: Révision de la chronologie de la déglaciation au Québec méridional. *Geogr. Phys. Quat.* **2003**, *57*, 115–138.
37. Gagné, S.; Larocque, M.; Pinti, D.L.; Saby, M.; Meyzonnat, G.; Méjean, P. Benefits and limitations of using isotope-derived groundwater travel times and major ion chemistry to validate a regional groundwater flow model: Example from the Centre-du-Québec region, Canada. *Can. Water Resour. J. Rev. Can. Ressour. Hydr.* **2017**, *43*, 195–213. [[CrossRef](#)]
38. Dubois, E.; Larocque, M.; Gagné, S.; Meyzonnat, G. Simulation of long-term spatiotemporal variations in regional-scale groundwater recharge: Contributions of a water budget approach in cold and humid climates. *Hydrol. Earth Syst. Sci.* **2021**, *25*, 6567–6589. [[CrossRef](#)]
39. Meyzonnat, G.; Larocque, M.; Barbecot, F.; Pinti, D.; Gagne, S. The potential of major ion chemistry to assess groundwater vulnerability of a regional aquifer in southern Quebec (Canada). *Environ. Earth Sci.* **2015**, *75*, 1–12. [[CrossRef](#)]
40. Cloutier, V.; Lefebvre, R.; Savard, M.M.; Bourque, É.; Therrien, R. Hydrogeochemistry and groundwater origin of the Basses-Laurentides sedimentary rock aquifer system, St. Lawrence Lowlands, Québec, Canada. *Appl. Hydrogeol.* **2005**, *14*, 573–590. [[CrossRef](#)]
41. Cloutier, V.; Lefebvre, R.; Savard, M.M.; Therrien, R. Desalination of a sedimentary rock aquifer system invaded by Pleistocene Champlain Sea water and processes controlling groundwater geochemistry. *Environ. Earth Sci.* **2010**, *59*, 977–994. [[CrossRef](#)]
42. Castro, M.C.; Ma, L.; Hall, C.M. A primordial, solar He–Ne signature in crustal fluids of a stable continental region. *Earth Planet. Sci. Lett.* **2009**, *279*, 174–184. [[CrossRef](#)]
43. Matsuda, J.; Matsumoto, T.; Sumino, H.; Nagao, K.; Yamamoto, J.; Miura, Y.; Kaneoka, I.; Takahata, N.; Sano, Y. The  $^3\text{He}/^4\text{He}$  ratio of the new internal He Standard of Japan (HESJ). *Geochem. J.* **2002**, *36*, 191–195. [[CrossRef](#)]
44. Pinti, D.L.; Van Drom, E. PALEOTEMP: A Mathematica<sup>®</sup> program for evaluating paleotemperatures from the concentration of atmosphere-derived noble gases in ground water. *Comput. Geosci.* **1998**, *24*, 33–41. [[CrossRef](#)]
45. Ballentine, C.; Hall, C. Determining paleotemperature and other variables by using an error-weighted, nonlinear inversion of noble gas concentrations in water. *Geochim. Cosmochim. Acta* **1999**, *63*, 2315–2336. [[CrossRef](#)]
46. Heaton, E.T.H.; Vogel, J.C. Excess Air in Groundwater. *J. Hydrol.* **1981**, *50*, 201–208. [[CrossRef](#)]
47. Fontes, J.-C.; Garnier, J.-M. Determination of the initial  $^{14}\text{C}$  activity of the total dissolved carbon: A review of the existing models and a new approach. *Water Resour. Res.* **1979**, *15*, 399–413. [[CrossRef](#)]
48. El-Kadi, A.I.; Plummer, L.N.; Aggarwal, P. NETPATH-WIN: An Interactive User Version of the Mass-Balance Model, NETPATH. *Ground Water* **2011**, *49*, 593–599. [[CrossRef](#)]
49. Clarke, W.; Jenkins, W.; Top, Z. Determination of tritium by mass spectrometric measurement of  $^3\text{He}$ . *Int. J. Appl. Radiat. Isot.* **1976**, *27*, 515–522. [[CrossRef](#)]
50. Smith, S.; Kennedy, B. The solubility of noble gases in water and in NaCl brine. *Geochim. Cosmochim. Acta* **1983**, *47*, 503–515. [[CrossRef](#)]
51. Craig, H.; Lupton, J.E.; Welhan, J.A.; Poreda, R. Helium isotope ratios in Yellowstone and Lassen Park volcanic gases. *Geophys. Res. Lett.* **1978**, *5*, 897–900. [[CrossRef](#)]
52. Benson, B.B.; Krause, D. Isotopic fractionation of helium during solution: A probe for the liquid state. *J. Solut. Chem.* **1980**, *9*, 895–909. [[CrossRef](#)]
53. IAEA/WMO. Global Network of Isotopes in Precipitation. The Gnip Database. 2004. Available online: <https://websso.iaea.org/> (accessed on 13 June 2022).
54. Méjean, P.; Pinti, D.L.; Kagoshima, T.; Roulleau, E.; Demarets, L.; Poirier, A.; Takahata, N.; Sano, Y.; Larocque, M. Mantle helium in Southern Quebec groundwater: A possible fossil record of the New England hotspot. *Earth Planet. Sci. Lett.* **2020**, *545*, 116352. [[CrossRef](#)]

55. Moritz, A.; Hélie, J.-F.; Pinti, D.L.; Larocque, M.; Barnetche, D.; Retailleau, S.; Lefebvre, R.; Gélinas, Y. Methane Baseline Concentrations and Sources in Shallow Aquifers from the Shale Gas-Prone Region of the St. Lawrence Lowlands (Quebec, Canada). *Environ. Sci. Technol.* **2015**, *49*, 4765–4771. [[CrossRef](#)]
56. Ma, L.; Castro, M.C.; Hall, C.M.; Walter, L.M. Cross-formational flow and salinity sources inferred from a combined study of helium concentrations, isotopic ratios, and major elements in the Marshall aquifer, southern Michigan. *Geochem. Geophys. Geosyst.* **2005**, *6*, Q10004. [[CrossRef](#)]
57. Buttitta, D.; Caracausi, A.; Chiaraluce, L.; Favara, R.; Gasparro, M.; Sulli, A. Continental Degassing of Helium in an Active Tectonic Setting (Northern Italy): The Role of Seismicity. *Sci. Rep.* **2020**, *10*, 162. [[CrossRef](#)]
58. Méjean, P.; Pinti, D.L.; Ghaleb, B.; Larocque, M. Fracturing-induced release of radiogenic  $^4\text{He}$  and  $^{234}\text{U}$  into groundwater during the last deglaciation: An alternative source to crustal helium fluxes in periglacial aquifers. *Water Resour. Res.* **2017**, *53*, 5677–5689. [[CrossRef](#)]
59. Torgersen, T.; Clarke, W. Helium accumulation in groundwater, I: An evaluation of sources and the continental flux of crustal  $^4\text{He}$  in the Great Artesian Basin, Australia. *Geochim. Cosmochim. Acta* **1985**, *49*, 1211–1218. [[CrossRef](#)]
60. Torgersen, T.; Ivey, G. Helium accumulation in groundwater. II: A model for the accumulation of the crustal  $^4\text{He}$  degassing flux. *Geochim. Cosmochim. Acta* **1985**, *49*, 2445–2452. [[CrossRef](#)]
61. Meynier, V.; O’Nions, R.K.; De Marsily, G.; Marty, B.; Torgersen, T. Helium isotope fluxes and groundwater ages in the Dogger Aquifer, Paris Basin. *Water Resour. Res.* **1993**, *29*, 1025–1035.
62. Kulongoski, J.; Hilton, D.R.; Izbicki, J.A. Source and movement of helium in the eastern Morongo groundwater Basin: The influence of regional tectonics on crustal and mantle helium fluxes. *Geochim. Cosmochim. Acta* **2005**, *69*, 3857–3872. [[CrossRef](#)]
63. Torgersen, T.; Clarke, W. Helium accumulation in groundwater, III. Limits on helium transfer across the mantle-crust boundary beneath Australia and the magnitude of mantle degassing. *Earth Planet. Sci. Lett.* **1987**, *84*, 345–355. [[CrossRef](#)]
64. Torgersen, T. Defining the role of magmatism in extensional tectonics: Helium 3 fluxes in extensional basins. *J. Geophys. Res. Earth Surf.* **1993**, *98*, 16257–16269. [[CrossRef](#)]
65. Torgersen, T. Continental degassing flux of  $^4\text{He}$  and its variability. *Geochem. Geophys. Geosyst.* **2010**, *11*, Q06002. [[CrossRef](#)]
66. Sano, Y.; Nakajima, J. Geographical distribution of  $^3\text{He}/^4\text{He}$  ratios and seismic tomography in Japan. *Geochem. J.* **2008**, *42*, 51–60. [[CrossRef](#)]
67. Ngoc, T.D.T.; Lefebvre, R.; Konstantinovskaya, E.; Malo, M. Characterization of deep saline aquifers in the Bécancour area, St. Lawrence Lowlands, Québec, Canada: Implications for  $\text{CO}_2$  geological storage. *Environ. Earth Sci.* **2014**, *72*, 119–146. [[CrossRef](#)]
68. Wang, M.; Wang, J.; Xu, G.; Zheng, Y.; Kang, X. Improved model for predicting the hydraulic conductivity of soils based on the Kozeny–Carman equation. *Water Policy* **2021**, *52*, 719–733. [[CrossRef](#)]
69. Chapuis, R.P.; Aubertin, M. On the use of the Kozeny–Carman equation to predict the hydraulic conductivity of soils. *Can. Geotech. J.* **2003**, *40*, 616–628. [[CrossRef](#)]
70. Méjean, P.; Pinti, D.L.; Larocque, M.; Ghaleb, B.; Meyzonnat, G.; Gagné, S. Processes controlling  $^{234}\text{U}$  and  $^{238}\text{U}$  isotope fractionation and helium in the groundwater of the St. Lawrence Lowlands, Quebec: The potential role of natural rock fracturing. *Appl. Geochem.* **2016**, *66*, 198–209. [[CrossRef](#)]
71. Comtois, P. Histoire holocène du climat et de la végétation à Lanoraie (Québec). *Can. J. Earth Sci.* **1982**, *19*, 1938–1952. [[CrossRef](#)]
72. Mott, R.J. Late-Pleistocene and Holocene palynology in southeastern Québec. *Geogr. Phys. Quat.* **2010**, *31*, 139–149.
73. Pickler, C.; Beltrami, H.; Mareschal, J.-C. Laurentide Ice Sheet basal temperatures during the last glacial cycle as inferred from borehole data. *Clim. Past* **2016**, *12*, 115–127. [[CrossRef](#)]
74. Pinti, D.L.; Marty, B. Separation of noble gas mixtures from petroleum and their isotopic analysis by mass spectrometry. *J. Chromatogr. A* **1998**, *824*, 109–117. [[CrossRef](#)]
75. Brennwald, M.S.; Schmidt, M.; Oser, J.; Kipfer, R. A Portable and Autonomous Mass Spectrometric System for On-Site Environmental Gas Analysis. *Environ. Sci. Technol.* **2016**, *50*, 13455–13463. [[CrossRef](#)]
76. McMurtry, G.M.; DaSilveira, L.A.; Horn, E.L.; Deluze, J.R.; Blessing, J.E. High  $^3\text{He}/^4\text{He}$  ratios in lower East Rift Zone steaming vents precede a new phase of Kilauea 2018 eruption by 8 months. *Sci. Rep.* **2019**, *9*, 11860. [[CrossRef](#)]